

Cite this: *J. Mater. Chem. A*, 2013, **1**, 12627

Plasmon-enhanced photocurrent in quasi-solid-state dye-sensitized solar cells by the inclusion of gold/silica core-shell nanoparticles in a TiO₂ photoanode†

Sanghyuk Wooh,^{‡ab} Yong-Gun Lee,^{‡c} Muhammad Nawaz Tahir,^d Donghoon Song,^c Michael Meister,^e Frédéric Laquai,^e Wolfgang Tremel,^d Juan Bisquert,^f Yong Soo Kang^{*c} and Kookheon Char^{*ab}

Direct evidence of the effects of the localized surface plasmon resonance (LSPR) of gold nanoparticles (Au NPs) in TiO₂ photoanodes on the performance enhancement in quasi-solid-state dye-sensitized solar cells (DSCs) is reported by comparing gold/silica core-shell nanoparticles (Au@SiO₂ NPs) and hollow silica nanoparticles with the same shell size of the core-shell nanoparticles. The Au nanoparticles were shelled by a thin SiO₂ layer to produce the core-shell structure, and the SiO₂ hollow spheres were made by dissolving the Au cores of the gold/silica core-shell nanoparticles. Therefore, the size and morphology of the SiO₂ hollow spheres were the same as the Au@SiO₂ NPs. The energy conversion efficiency was improved nearly 36% upon incorporating the Au nanoparticles, mostly due to the increase in J_{sc} , while V_{oc} and FF were unchanged. The improvement was mostly contributed by the LSPR of the Au@SiO₂ NPs, whereas the other parameters, such as the electron lifetime and electron diffusion coefficient, were nearly unchanged. Therefore, LSPR is an effective tool in improving the photocurrent and consequently the performance of DSCs.

Received 1st May 2013
Accepted 21st August 2013

DOI: 10.1039/c3ta11712j

www.rsc.org/MaterialsA

Introduction

Dye-sensitized solar cells (DSCs) have currently received much attention due to several advantages, such as the low fabrication cost and high power conversion efficiency greater than 12% under 1 sun illumination condition.^{1–4} The most widely studied DSC is comprised of an electrolyte sandwiched between two electrodes coated on a transparent conducting glass, such as

fluorine-doped tin oxide (FTO) glass; a photoanode and counter electrode. The photoanode consists of a mesoporous semiconductor such as a TiO₂ layer with sensitizers, whereas a typical counter electrode is made of a reduction catalyst such as platinum coated onto FTO. Upon light illumination, dye sensitizers adsorbed to the surface of the mesoporous TiO₂ layer generate electrons, which are subsequently injected into the TiO₂ layer for electricity production. Therefore, light absorption by sensitizers on the photoanodes plays a major role in determining the overall energy conversion efficiency of DSCs. A large body of research has been conducted to enhance the light harvesting efficiency in TiO₂ photoanodes. In this context, the development of more efficient dye sensitizers, including organic dyes with a higher extinction coefficient^{5,6} and energy-relay dyes,⁷ and their effective utilization methods, such as cocktail dye^{8,9} and selective dye adsorption^{10,11} concepts, have prevailed. In addition, the introduction of a scattering layer and inverse opal nanostructures are also common.^{12–14}

The localized surface plasmon resonance (LSPR) phenomena of metal nanoparticles has also been investigated to enhance light harvesting efficiency.^{15–17} The LSPR, which refers to the resonance between the electromagnetic field and free-electron oscillation, amplifies the electromagnetic field near the metal nanoparticles, resulting in plasmon enhanced light absorption of dye sensitizers in DSCs.^{18–23} The Hupp group first reported plasmon enhanced light harvesting in DSCs using silver

^aIntelligent Hybrids Research Center, Seoul National University, Seoul, 151-744, Korea. E-mail: khchar@plaza.snu.ac.kr; Tel: +82 2 880 1877

^bThe WCU program for Chemical Convergence for Energy and Environment, School of Chemical and Biological Engineering, Seoul National University, Seoul, 151-744, Korea

^cThe WCU Department of Energy Engineering and Center for Next Generation Dye-Sensitized Solar Cells, Hanyang University, Seoul 133-791, Korea. E-mail: kangys@hanyang.ac.kr; Tel: +82 2 2220 2336

^dInstitute of Inorganic Chemistry and Analytical Chemistry, Johannes Gutenberg-University, Duesbergweg 10-14, D-55099 Mainz, Germany

^eMax Planck Research Group for Organic Optoelectronics, Max-Planck-Institute for Polymer Research, Mainz, Germany

^fPhotovoltaics and Optoelectronic Devices Group, Departament de Física, Universitat Jaume I, 12071 Castelló, Spain

† Electronic supplementary information (ESI) available: Device characterization with incident-modulated photovoltage spectroscopy (IMVS) and incident-modulated photocurrent spectroscopy (IMPS). See DOI: 10.1039/c3ta11712j

‡ These authors contributed equally to this work.

nanoparticles on flat TiO₂ film, demonstrating considerable potential to increase the photocurrent.^{24,25} The photocurrent and power conversion efficiency of the DSC increased nearly 6–7-fold upon incorporating silver nanoparticles into a dye monolayer on the flat TiO₂ film (J_{sc} from 14.6 to 85.7 $\mu\text{A cm}^{-2}$, from 0.007 to 0.045%). Recently, enhanced charge carrier generation in solid-state DSCs was demonstrated by the LSPR effects of Au NPs coated on a mesoporous TiO₂ photoanode²⁶ and a hexagonal array of Ag nanodome-structured counter electrode.²⁷

Direct effects of LSPR by metallic nanoparticles on the performance of DSCs may not be readily evaluated in common I⁻/I₃⁻ redox couples which dissolve metallic nanoparticles, such as gold, by the following reaction:²⁸



One way to avoid the dissolution problem of metallic nanoparticles is to create a shell with an inert material, such as SiO₂. In this study, Au@SiO₂ NPs were synthesized in a solution process and mixed with a TiO₂ paste to fabricate Au@SiO₂ NPs incorporated mesoporous TiO₂ photoanodes. In addition, we used polyethylene glycol (PEG) based electrolyte to achieve stability of the Au core, inhibiting interaction between the Au core of Au@SiO₂ NPs and I⁻/I₃⁻ ions in the electrolyte. However, the properties of the core-shell nanoparticle-incorporated photoanodes were affected by both the metal cores and shell. Thus, the effects of the shell material on the cell performance must be considered. Until recently, even though a number of researches have been presented to improve the cell performance by utilizing the LSPR effects with metal/TiO₂ or SiO₂ core-shell structures, the quantitative analyses of the LSPR by metal cores and other changes in the photoanodes by shells are still difficult to separately evaluate.^{24–26} This problem may be solved by comparing the results of the same photoanode structures with and without core metal: core-shell and hollow shell. The hollow shell structure can be prepared by dissolving the core metal of the core-shell sphere by the dissolution reaction with I⁻/I₃⁻, which readily diffuses through a shell layer, such as SiO₂.²⁹ In this context, SiO₂ hollow spheres-incorporated TiO₂ photoanode was fabricated to quantify the effects of the LSPR clearly by the Au nanoparticles without disturbing the shell properties or structure. The TiO₂ photoanodes incorporating SiO₂ hollow spheres have the same morphology as the initial TiO₂ photoanodes incorporating Au@SiO₂ NPs, which is helpful for accurate comparison of photoanodes with and without LSPR. Through this novel approach, the LSPR effect in DSCs can be independently demonstrated with the effect of SiO₂ shells, such as the charge injection problem from dyes into the SiO₂ shell and the change of morphology and resistance.

Experimental

Materials

All chemicals were used without further purification, and water was doubly ionized. The chemicals used for the synthesis of Au@SiO₂ NPs, hydrogen tetrachloroaurate(III) trihydrate (HAuCl₄·3H₂O), hexadecyltrimethylammonium bromide

(CH₃(CH₂)₁₅N(Br)(CH₃)₃), sodium citrate (HOC(COONa)-(CH₂COONa)₂·2H₂O), ascorbic acid (C₆H₈O₆), (3-mercaptopropyl)trimethoxysilane (HS(CH₂)₃Si(OCH₃)₃) and a sodium silicate solution (Na₂O(SiO₂)_x·xH₂O) were purchased from Sigma-Aldrich. For the fabrication of the dye-sensitized solar cells, polyethyleneglycol dimethylether (PEGDME, M_w : 500), 1-methyl-3-propylimidazoliumiodide (MPII), iodine (I₂) and fumed silica (~14 nm) were obtained from Sigma-Aldrich. TiO₂ paste (DSL 18NR-T) and sensitizer dye, *cis*-dithiocyanato-bis(2,2'-bipyridyl-4,4'-dicarboxylato)ruthenium(II) bis(tetrabutylammonium) (N719), were purchased from Dyesol.

Synthesis of gold nanoparticles

Au NPs were prepared using a seed-mediated method.³⁰ First, 15 nm-diameter Au NP seeds were synthesized *via* citrate reduction. In a typical procedure, 10 ml of a 1 mM gold(III) chloride trihydrate aqueous solution was refluxed at boiling temperature under vigorous stirring, followed by the quick injection of 1 ml of a 39 mM sodium citrate solution. After 15 min, the heating was stopped, and the reaction contents were cool to room temperature. To make larger nanoparticles, a 2 ml seed particle solution was added to 100 ml of a 0.5 mM gold(III) chloride trihydrate aqueous solution containing 0.03 M CTAB and 1 mM ascorbic acid. The solution was reacted for 4 hours, and the product was collected using centrifugation (9000 rpm, at room temperature for 10 min).

Synthesis of gold/silica core-shell nanoparticles

Au@SiO₂ NPs were synthesized by a modified procedure previously reported by Obare *et al.*²⁹ In this method, growth of silica was performed after surfactant substitution with a silane coupling group, (3-mercaptopropyl)trimethoxysilane (MPTMS). MPTMS in ethanol was added to the Au NPs solution. After three hours, an aqueous sodium silicate solution was added and reacted for three additional days. The contents were purified several times by precipitation using centrifugation and were re-dispersed in ethanol.

Paste preparation

As-prepared Au@SiO₂ NPs dispersed in ethanol were added and well mixed with the commercial titanium dioxide (TiO₂) paste with an average size of 20 nm (DSL 18NR-T, Dyesol). In order to achieve the same thickness of photoanodes after sintering, excess ethanol from the paste was evaporated using nitrogen to produce a homogenous concentration of paste materials.

Device fabrication

For the formation of an electron blocking layer between the FTO substrate and oxidized species in the electrolyte, 0.1 M of Ti(IV) bis(ethyl acetoacetato)diisopropoxide in a 1-butanol solution was spin-coated on FTO glass (TEC 8, Pilkington) followed by sintering at 500 °C. TiO₂ photoanodes were fabricated on the blocking layer with TiO₂ paste using a doctor blade method followed by sintering at 500 °C for 15 min. Subsequently, TiO₂ nanostructure-coated FTO substrates were dipped into 40 mM

TiCl₄ in H₂O solution at 70 °C for 30 min and sintered at 500 °C for 15 min.

TiO₂ photoanodes were dipped into the 0.3 mM N719 dye (*cis*-bis(isothiocyanato)bis(2,2'-bipyridyl-4,4'-dicarboxylato) ruthenium(II) bis-tetrabutylammonium, Dyesol) in an acetonitrile and *tert*-butanol solution (1 : 1 v/v) at 30 °C for 18 hours and then rinsed with acetonitrile and dried using a stream of nitrogen. A Pt counter electrode was prepared by thermal decomposition of 0.01 M H₂PtCl₆ in an isopropyl alcohol solution on the FTO substrate followed by sintering at 500 °C for 30 min. After loading the dyes onto the TiO₂ electrodes, Surlyn (25 μm, Solaronix) was attached to the TiO₂ photoanode as a spacer. The polymer electrolyte was spread on the spacer gap, and the Pt counter electrode was placed on top.

The electrolyte consists of poly(ethylene glycol dimethyl ether) (PEGDME) (*M_w*: 500, Sigma-Aldrich), 1-methyl-3-propylimidazolium iodide (MPII, Sigma-Aldrich), iodine (I₂, Sigma-Aldrich), and fumed silica nanoparticles (14 nm, Sigma-Aldrich). The composition of [–O–][MPII]–[I₂] was 10 : 1 : 0.1, and the silica NPs were 9 wt% of the total polymer electrolyte.³¹

Solar cell characterization

The thickness of TiO₂ films was characterized with a surface profiler (alpha-step IQ, Tencor) and field emission scanning electron spectroscopy (JSM-6701F, JEOL). Absorption properties of photoanodes were measured by UV-Vis spectroscopy (V-670 UV-Vis spectrophotometer, Jasco) with an integrating sphere. Current–voltage characterization of the DSCs was performed with a Keithley 2400 digital source meter and solar simulator equipped with a 300 W Xenon arc-lamp (Newport) under a 1 sun illumination (AM 1.5, 100 mW cm^{–2}). The light intensity was calibrated by a silicon solar cell (PV measurement). In addition, the quantum efficiency of DSCs was analyzed by an incident photon to current efficiency (IPCE) (PV measurements, Inc.) as a function of wavelength. The charge transfer resistance and electron lifetime in the photoanodes were characterized by electrochemical impedance spectroscopy (EIS) using an IM6 (Zahner) under dark conditions with a bias potential of –0.54 V. The frequency was in the range of 1 MHz to 0.1 Hz, and the amplitude was fixed to 10 mV. The obtained spectra were fitted and analyzed using Z-View software with equivalent circuits.

The electron diffusion coefficient and electron lifetime of the photoanodes were evaluated by intensity-modulated photocurrent spectroscopy (IMPS) under short-circuit conditions and intensity-modulated photovoltage spectroscopy (IMVS) under open-circuit conditions as a function of light intensity using a controlled intensity modulated photo spectroscopy (CIMPS) system (Zahner) and a white light source (Zahner). The detailed measurement conditions are described elsewhere.³²

Results and discussion

Fig. 1a–c show TEM images of three, differently sized Au NPs shelled with thin SiO₂ (Au@SiO₂ NPs). The average diameter of Au NPs obtained by varying the concentration of the Au precursor was (a) 30, (b) 50, and (c) 160 nm. Subsequently, their

surfaces were modified with 3-mercaptopropyl trimethoxysilane (MPTMS), and the thickness of the SiO₂ shells were controlled to approximately 11 nm by adding an aqueous sodium silicate solution.

Even though the Au NPs were protected by the SiO₂ shell, the Au cores were dissolved by contact with I[–]/I₃[–] ions penetrating the thin silica shell in a few hours. Therefore, the SiO₂ shell was treated with TiCl₄ to block the penetration of I[–]/I₃[–] ions and consequently improve the stability of the Au core nanoparticles against dissolution. In addition, a poly(ethylene glycol) dimethylether (PEGDME, *M_w*: 500)-based polymer electrolyte, instead of typical acetonitrile-based liquid electrolytes, was used for quasi-solid-state DSCs in order to retard the possible penetration of the I[–]/I₃[–] ions through the SiO₂ shell. Based on our experimental results, a SiO₂ shell thinner than 8 nm hardly protected the Au core from the electrolyte contact, even though high *M_w* PEGDME was applied as a viscous solvent for quasi-solid electrolytes. Experimental data suggests that 10 nm was the minimum thickness of the SiO₂ shell necessary to protect the Au core from the dissolution.

The localized surface plasmon resonance (LSPR) effects of Au@SiO₂ NPs by varying the Au core size were characterized using UV-vis spectroscopy, as shown in Fig. 1d. The absorption peak appears at 537, 547, and 565 nm for Au@SiO₂ NPs with the size of the Au core/SiO₂ shell 30/12, 50/11, and 160/10 nm, respectively. This shift in the absorption band is attributed to the change in the oscillation frequency of LSPR caused by varying the average diameter of the Au NPs. The absorption band of LSPR shifts to a longer wavelength by increasing the size of Au NPs as a result of the decrease in the oscillation frequency. The coupling between the LSPR of the Au NPs and the absorption of dyes is one of the key factors for the enhanced performance of DSCs using Au NPs. In this case, the absorption peak difference or coupling wavelength mismatch of Au NPs (160 nm) with respect to the N719 dyes was ~40 nm, as shown

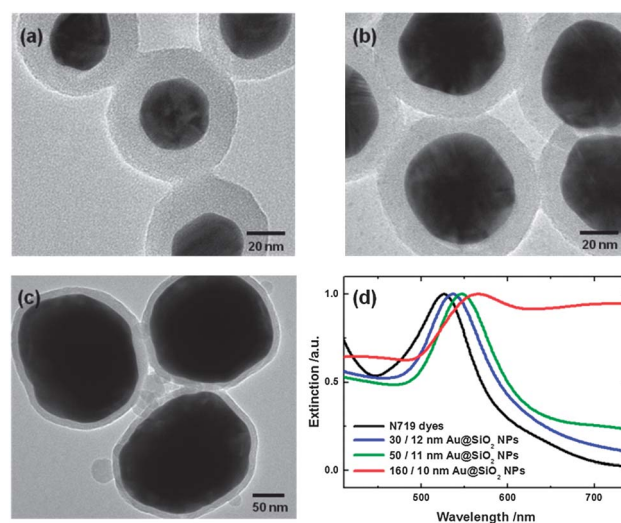


Fig. 1 Transmission electron spectroscopy (TEM) of various sizes of Au@SiO₂ NPs; (a) 30/12 nm, (b) 50/11 nm, and (c) 160/10 nm. (d) Normalized UV-vis spectrum of the N719 dyes and the Au@SiO₂ NPs in ethanol.

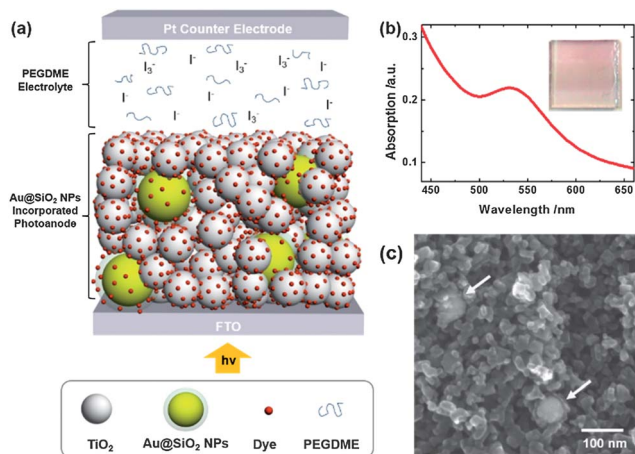


Fig. 2 (a) Schematic illustration of Au@SiO₂ NP-incorporated photoanode in PEGDME-based quasi-solid-state DSC. (b) UV-vis spectrum, photograph and (c) cross-sectional scanning electron microscopy (SEM) image of Au@SiO₂ NP-incorporated photoanode with ~20 nm diameter TiO₂ nanoparticles (white arrows indicate Au@SiO₂ NPs).

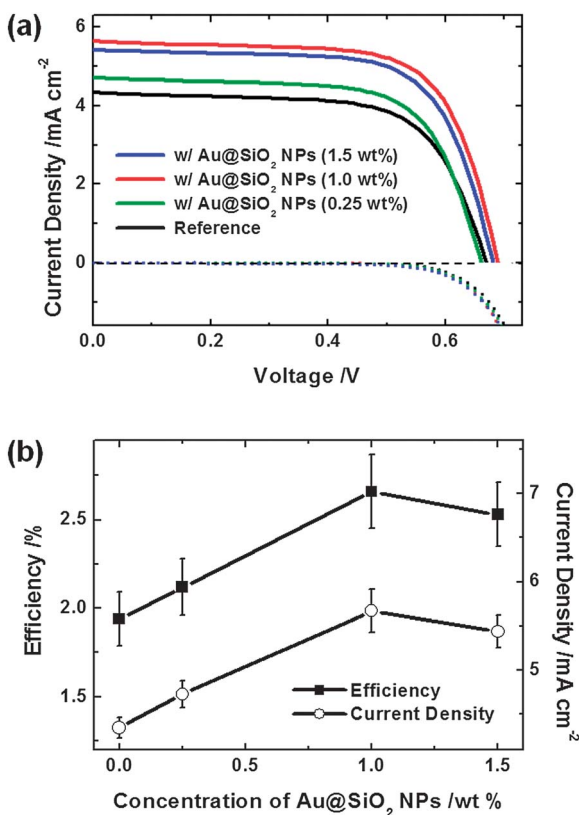


Fig. 3 (a) Photocurrent–voltage characteristics of DSCs with different concentrations of Au@SiO₂ NPs under illumination (continuous lines) and dark (dotted lines). (b) Power conversion efficiency (closed squares) and short circuit current density (open circles) versus the concentration of Au@SiO₂ NPs. The error bars indicate the variation of the values for 7 independent measurements for each cell.

in Fig. 1(d). Additionally, when larger Au NPs were incorporated into the TiO₂ photoanodes, Mie scattering which is a long range effect should occur and it can be mixed with the effect of LSPR.

Alternatively, as the size of the Au NPs increases, the field enhancement is more widely developed, leading to increased light harvesting of the dyes. Therefore, 50/11 nm Au@SiO₂ NPs were chosen for the fabrication of photoanodes to investigate the effects of LSPR in DSCs considering their coupling wavelength mismatch, the change in surface area, and the near-field enhancement effects.

Fig. 2a shows the schematic illustration of a Au@SiO₂ NP-incorporated TiO₂ photoanode. The LSPR of Au@SiO₂ NPs in TiO₂ photoanodes was observed by the reddish photoanode (inset photograph) and by the UV-vis spectrum, as shown in Fig. 2b. Fig. 2c shows Au@SiO₂ NPs in the photoanodes surrounded by TiO₂ NPs using scanning electron microscopy (SEM). Noticeably, the shapes of the Au@SiO₂ NPs were unchanged after sintering at 500 °C.

The photocurrent–voltage characteristics of DSCs with TiO₂ photoanodes incorporating Au@SiO₂ NPs are represented in Fig. 3. The film thickness of photoanodes with and without Au@SiO₂ NPs was adjusted to 2 μm to more clearly characterize the effects of LSPR, which is thinner than a conventional TiO₂ layer (Fig. S1†). In order to optimize the incorporation of Au@SiO₂ NPs for DSC performance, the concentration of Au@SiO₂ NPs in the TiO₂ paste was varied from 0.25 to 1.5 wt%. The short circuit current density (J_{sc}) was increased upon the incorporation of Au@SiO₂ NPs, while the open-circuit voltage (V_{oc}) and fill factor (FF) remained nearly unchanged. The J_{sc} and power conversion efficiency (PCE) of DSCs with the addition of 1.0 wt% of Au@SiO₂ NPs into the TiO₂ layer were increased to 5.67 mA cm⁻² and 2.66%, respectively, with respect to the same thickness reference TiO₂ photoanode without Au@SiO₂ NPs (4.35 mA cm⁻², 1.94%). However, at concentrations greater than 1.0 wt% Au@SiO₂ NPs, the J_{sc} (5.44 mA cm⁻²) and PCE (2.53%) were slightly decreased, as shown in Fig. 3b and Table 1. The inclusion of Au@SiO₂ NPs in the photoanode may have possible side effects. First, the Au@SiO₂ NPs could inhibit the light absorption of dyes in the photoanodes while the Au@SiO₂ NPs in the photoanodes absorb the incident light as well as dyes but without converting photons to charges.²⁶ On that account, the light harvesting efficiency may slightly decrease when the concentration of Au@SiO₂ NPs in the photoanode becomes higher than the critical point. Secondly, Au@SiO₂ NPs with a size of ~70 nm decrease the total amount of dye loading in the photoanodes due to the smaller surface area relative to 20 nm TiO₂ NPs. Finally, it is difficult to inject electrons from the excited dyes into the insulator SiO₂ shell. These side effects of the inclusion of Au@SiO₂ NPs may result in a decrease in photocurrent and consequently the photovoltaic performance of DSCs to a small extent. However, the overall energy conversion efficiency increased from 1.94 to 2.66%, which was a nearly 30% improvement, suggesting that the positive effects of LSPR are significant. Therefore, the performance was further characterized in the following sections. In order to evaluate the quantitative effects of LSPR from Au cores excluding the SiO₂ shell effects, the Au@SiO₂ NP-incorporated photoanodes with and without the Au cores were compared. Experimentally, TiO₂ photoanodes incorporating SiO₂ hollow spheres with the same size of Au@SiO₂ NP shell but without the Au core were

Table 1 I - V characteristics of the DSCs with TiO_2 photoanodes employing Au@SiO_2 NPs and SiO_2 hollow spheres^a

Type of TiO_2 photoanode	Concentration of Au@SiO_2 NPs (wt%)	V_{oc} (V)	J_{sc} (mA cm^{-2})	FF (%)	Efficiency (%)
Reference (only TiO_2)	—	0.664	4.35	67.0	1.94
TiO_2 w/ Au@SiO_2 NPs	0.25	0.657	4.73	67.8	2.12
	1.0	0.684	5.67	68.6	2.66
	1.5	0.676	5.44	68.7	2.53
w/ SiO_2 hollow spheres	1.0	0.665	4.4	67.7	1.97

^a The thickness of TiO_2 photoanodes are adjusted with 2 μm ; measured under 1 sun condition (AM 1.5 , 100 mW cm^{-2}) with 0.25 cm^2 active area.

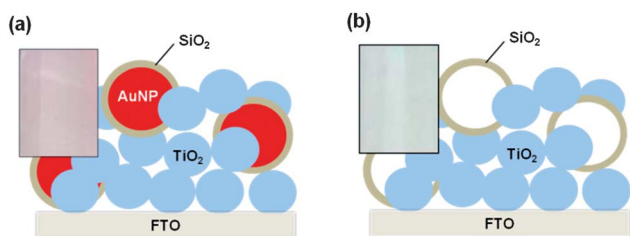


Fig. 4 Schemes of the TiO_2 photoanodes incorporating (a) Au@SiO_2 NPs and (b) SiO_2 hollow spheres. Photographs of the corresponding photoanodes are shown in the insets.

introduced by dipping Au@SiO_2 NP-incorporated photoanodes in an I^-/I_3^- liquid electrolyte for a few hours, which has the same morphology and thickness of the photoanode with Au@SiO_2 NPs. As expected, the SiO_2 hollow sphere was formed without a change in morphology due to the exclusive dissolution reaction eqn (1) of Au with I^-/I_3^- ions, which was easily demonstrated by the disappearance of the reddish color and characterized by scanning electron microscopy, as shown by the inset photographs of Fig. 4 and S2(a).[†] Fig. 5a shows the decreased light absorption of N719 dyes upon incorporating the SiO_2 hollow spheres rather than Au@SiO_2 NPs, indicating the effects of the presence of Au cores. The amount of dyes adsorbed on the TiO_2 surface were characterized and this result shows that the dyes loaded in SiO_2 hollow sphere incorporated photoanodes are nearly the same as the amount in the Au@SiO_2 NPs incorporated photoanode (Fig. S2(c)).[†] The only difference between these photoanodes was the Au cores, suggesting that

the enhanced light absorption is primarily attributed to the LSPR effects of the Au core. In order to confirm the LSPR effect more distinctly, we characterized absorption spectrum of the photoanodes additionally with N749 dyes (green dye) which absorb longer wavelength of light ($>600 \text{ nm}$) compare to Au NPs ($\sim 530 \text{ nm}$), as shown in Fig. 5a. Through the distinguished peaks of LSPR and light absorption of N749 dyes, the effect of LSPR on the enhanced light absorption of dyes was clearly verified. Moreover, almost the same reflectance of Au@SiO_2 NPs and SiO_2 hollow spheres incorporated photoanodes were characterized by UV-vis spectroscopy with an integrating sphere and both photoanodes show only $\sim 2\%$ off-specular reflection by scattered light (Fig. S3[†]). This provides convincing evidence that absorption enhancement was mainly induced by LSPR which is near-field effect and not Mie scattering which is far-field effect.

Fig. 5b shows the photocurrent-voltage (J - V) characteristics of DSCs that are consistent with the results obtained from the difference in the light absorption, as shown in Fig. 5a. DSCs based on the TiO_2 photoanode incorporating Au@SiO_2 NPs exhibited $\sim 28\%$ greater J_{sc} and PCE than those with the hollow SiO_2 spheres. The increase of J_{sc} agrees well with the incident photon-to-current efficiency (IPCE) results, and the difference obtained by subtracting IPCE values increased at the same wavelength as the absorption band of LSPR (Fig. 5c). Moreover, the photoanode incorporating SiO_2 hollow spheres shows similar J_{sc} of 4.4 mA cm^{-2} and PCE of 1.97% with respect to the reference TiO_2 photoanode, as summarized in Table 1. For the photoanodes incorporating SiO_2 hollow spheres, only the Au cores were removed from the Au@SiO_2 NPs photoanode, while

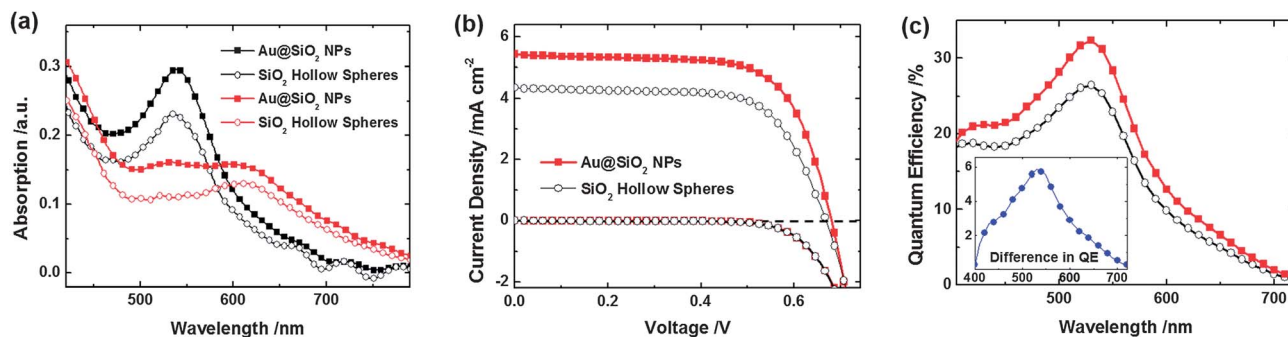


Fig. 5 (a) UV-vis spectrum of TiO_2 photoanodes with N719 dyes (black lines) and N749 dyes (red lines). (b) Photocurrent-voltage characteristics and (c) IPCE spectrum of DSCs characterized with the inclusion of Au@SiO_2 NPs (the red closed squares) and SiO_2 hollow spheres (the black open circles). Devices had 2 μm of the TiO_2 films and photovoltaic performance was measured under 1 sun condition (AM 1.5 , 100 mW cm^{-2} solar illumination) with 0.25 cm^2 active area.

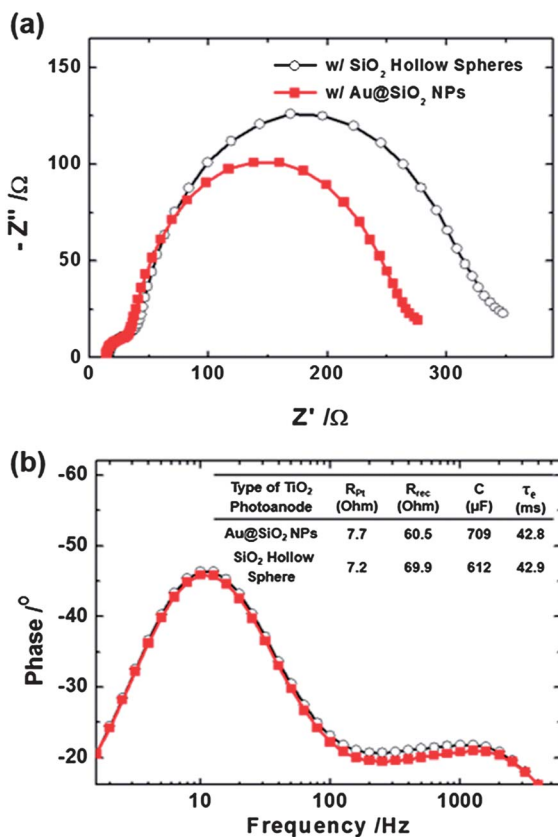


Fig. 6 Impedance spectra of DSCs with photoanodes incorporating Au@SiO₂ NPs (closed squares) and SiO₂ hollow spheres (open circles) in the dark condition with a bias potential of -0.54 V ((a) Nyquist plot and (b) Bode plot). Charge transfer resistance (R_{pt}), recombination resistance (R_{rec}), capacitance (C) and electron lifetime (τ_e) of photoanodes are shown in the inset table.

the surface area and morphology of the TiO₂ photoanode were unchanged. Thus, the small change of the photovoltaic performance between the reference and SiO₂ hollow sphere photoanodes suggested that the effects of the changes in surface area and morphology upon incorporating Au@SiO₂ NPs on the cell performance were nearly negligible. The performance enhancement upon incorporating Au@SiO₂ NPs into a photoanode is mostly due to the LSPR effects of the Au nanoparticles.

Electrochemical impedance spectroscopy (EIS) was performed in dark conditions with a bias potential of -0.54 V (Fig. 6) to characterize the cell performance, and the performance parameters were obtained by fitting with the general transmission model of DSCs.³³ In Fig. 6a, the Nyquist plots show two semicircles. The first semicircle at high frequency was attributed to the charge transfer resistance at the Pt counter electrode–polymer electrolyte interface (R_{pt}), and the second semicircle at mid-frequency was associated with the electron recombination resistance (R_{rec}) and capacitance (C) at the TiO₂–polymer electrolyte interface. For Bode plots, the characteristic frequency peak in the mid-frequencies was unchanged (Fig. 6b), indicating nearly the same electron lifetimes for the two samples. The values are listed in the inset table of Fig. 6b.

The roles of the Au@SiO₂ NPs in the electron lifetime and the electron diffusion coefficient in the TiO₂ photoanodes were also

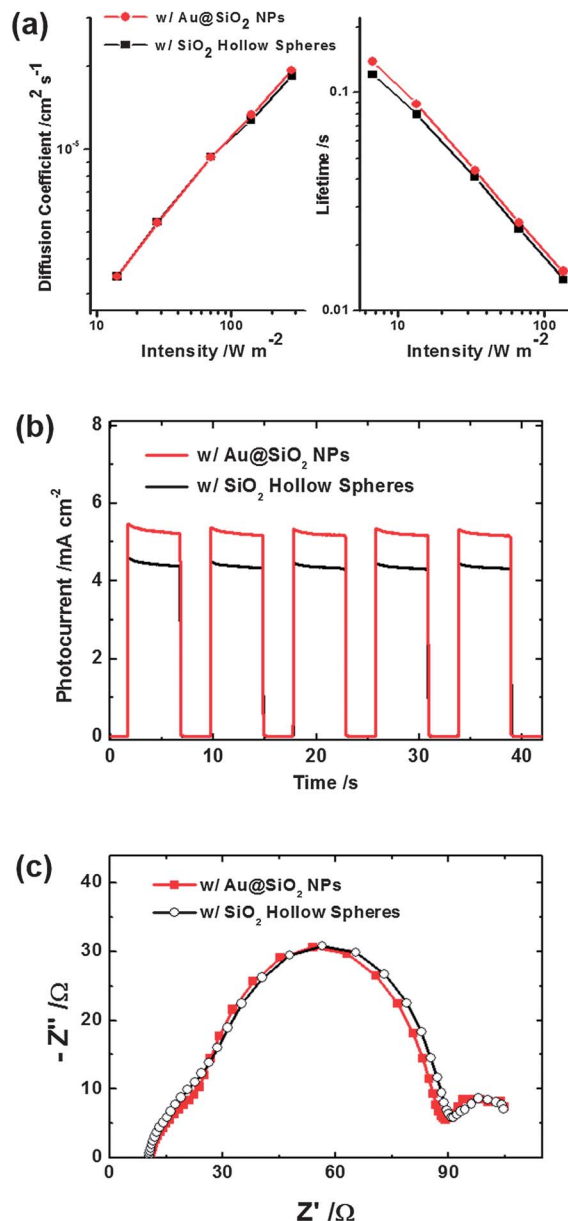


Fig. 7 (a) The electron diffusion coefficient (left) and the electron lifetime (right) determined by incident-modulated photocurrent spectroscopy (IMPS) and incident-modulated photovoltage spectroscopy (IMVS) as a function of light intensity, respectively. (b) Photocurrent transient measurement results and (c) impedance spectra of DSCs with photoanodes incorporating Au@SiO₂ NPs and SiO₂ hollow spheres. Impedance spectrum was characterized under illumination with bias potential of -0.65 V.

evaluated with incident-modulated photovoltage spectroscopy (IMVS) and incident-modulated photocurrent spectroscopy (IMPS) as a function of the light intensity given in Fig. 7a. In accordance with the EIS measurements, the electron lifetime upon the inclusion of the Au@SiO₂ NPs was unchanged compared to that of the photoanode with the hollow SiO₂ spheres. Furthermore, the electron diffusion coefficient was also unchanged, and thus the diffusion lengths (L_n , $L_n = (D_n \tau_n)^{1/2}$) derived from these values were almost same between the photoanodes containing Au@SiO₂ NPs with and without the

Au core nanoparticles. In addition, the transient photocurrent and the diffusion coefficients of electrolyte ($D[\text{I}_3^-]$) were measured, as shown in Fig. 7b and c. Nearly the same values of Au@SiO₂ NPs ($2.36 \times 10^{-7} \text{ cm}^2 \text{ s}^{-1}$) and hollow SiO₂ spheres ($2.38 \times 10^{-7} \text{ cm}^2 \text{ s}^{-1}$) incorporated photoanodes were evaluated. These results reveal that despite the enhanced light absorption of photoanodes by LSPR, the Au NPs had no influence on the electrochemical properties in the photoanodes and electrolyte due to the presence of the insulating layer inhibiting interaction between Au cores and electrolyte.

Conclusions

Au@SiO₂ NPs incorporated into a conventional mesoporous TiO₂ photoanode resulted in a significant increase in the energy conversion efficiency (up to 36% from 1.94 to 2.66% with a 2 μm-thick photoanode under 1 sun illumination condition) in quasi-solid state DSCs, mostly due to the enhanced photocurrent density from 4.35 to 5.67 mA cm⁻² by the LSPR effects of the Au NPs. In addition, the LSPR effects were directly observed by comparing results between the Au@SiO₂ NPs- and SiO₂ hollow spheres-incorporated TiO₂ photoanodes, where the hollow spheres were obtained by dissolving the Au core with I⁻/I₃⁻ ions and had same morphologies as Au@SiO₂ NPs. The influences from LSPR of the Au core in optical, electrochemical, and photovoltaic properties of the photoanodes were characterized by UV-vis spectroscopy and EIS measurements separate from the effect of SiO₂ shell and morphology change. From this, we demonstrated that the incorporation of the Au@SiO₂ NPs enhanced the light harvesting efficiency of dye molecules without changing the electron lifetime and diffusion coefficient of the TiO₂ photoanodes and were very effective in improving the power conversion efficiency of DSCs.

Acknowledgements

S. Wooh[‡] and Y. Lee[‡] contributed equally to this work. This work was financially supported by the National Creative Research Initiative Center for Intelligent Hybrids (No. 2010-0018290) through the National Research Foundation of Korea (NRF) grant funded by the Korea government (MSIP). This work was also in part supported by the International Research Training Group (IRTG): Self Organized Materials for Optoelectronics, jointly supported by the DFG (Germany) and NRF (Korea). Additionally, this work was supported by the National Research Foundation of Korea (NRF) grant funded by the Korea government (MSIP) for the Center for Next Generation Dye-sensitized Solar Cells (No. 2013004800).

Notes and references

- 1 B. O'Regan and M. Grätzel, *Nature*, 1991, **353**, 737.
- 2 M. Grätzel, *Nature*, 2001, **414**, 338.
- 3 M. K. Nazeeruddin, F. D. Angelis, S. Fantacci, A. Selloni, G. Viscardi, P. Liska, S. Ito, B. Takeru and M. Grätzel, *J. Am. Chem. Soc.*, 2005, **127**, 16835.
- 4 A. Yella, H.-W. Lee, H. N. Tsao, C. Yi, A. K. Chandiran, M. K. Nazeeruddin, W. W.-G. Diao, C.-Y. Yeh, S. M. Zakeeruddin and M. Grätzel, *Science*, 2011, **334**, 629.
- 5 C.-Y. Chen, M. Wang, J.-Y. Li, N. Pootrakulchote, L. Alibabaei, C.-H. Ngoc-le, J.-D. Decoppet, J.-H. Tsai, C. Grätzel, C.-G. Wu, S. M. Zakeeruddin and M. Grätzel, *ACS Nano*, 2009, **3**, 3103.
- 6 N. Cai, S.-J. Moon, L. Cevey-Ha, T. Moehl, R. Humphry-Baker, P. Wang, S. M. Zakeeruddin and M. Grätzel, *Nano Lett.*, 2011, **11**, 1452.
- 7 B. E. Hardin, E. T. Hoke, P. B. Armstrong, J. H. Yum, P. Comte, T. Torres, J. M. J. Frechet, M. K. Nazeeruddin, M. Grätzel and M. D. McGehee, *Nat. Photonics*, 2009, **3**, 406.
- 8 W. Zhao, Y. J. Hou, X. S. Wang, B. W. Zhang, Y. Cao, R. Yang, W. B. Wang and X. R. Xiao, *Sol. Energy Mater. Sol. Cells*, 1999, **58**, 173.
- 9 J.-H. Yum, S.-R. Jang, P. Walter, T. Geiger, F. Nüesch, S. Kim, J. Ko, M. Grätzel and M. K. Nazeeruddin, *Chem. Commun.*, 2007, 4680.
- 10 K. Lee, S. W. Park, M. J. Ko, K. Kim and N.-G. Park, *Nat. Mater.*, 2009, **8**, 665.
- 11 J.-H. Yum, E. Baranoff, S. Wenger, M. K. Nazeeruddin and M. Grätzel, *Energy Environ. Sci.*, 2011, **4**, 842.
- 12 S.-H. A. Lee, N. M. Abrams, P. G. Hoertz, G. D. Barber, L. I. Halaoui and T. E. Mallouk, *J. Phys. Chem. B*, 2008, **112**, 14415.
- 13 J.-H. Shin and J. H. Moon, *Langmuir*, 2011, **27**, 6311.
- 14 S.-H. Han, S. Lee, H. Shin and H. S. Jung, *Adv. Energy Mater.*, 2011, **1**, 546.
- 15 Y. A. Akimov, K. Ostrikov and E. P. Li, *Plasmonics*, 2009, **4**, 107.
- 16 Y. A. Akimov, W. S. Koh and K. Ostrikov, *Opt. Express*, 2009, **17**, 10195.
- 17 S.-S. Kim, S.-I. Na, J. Jo, D.-Y. Kim and Y.-C. Nah, *Appl. Phys. Lett.*, 2008, **93**, 073307.
- 18 B. Ding, B. J. Lee, M. Yang, H. S. Jung and J.-K. Lee, *Adv. Energy Mater.*, 2011, **1**, 415.
- 19 J. Qi, X. Dang, P. T. Hammond and A. M. Belcher, *ACS Nano*, 2011, **5**, 7108.
- 20 S. W. Sheehan, H. Noh, G. W. Brudvig, H. Cao and C. Schmittenmaer, *J. Phys. Chem. C*, 2013, **117**, 927.
- 21 H. Choi, W. T. Chen and P. V. Kamat, *ACS Nano*, 2012, **6**, 4418.
- 22 D. Zhang, M. Wang, A. G. Brolo, J. Shen, X. Li and S. Huang, *J. Phys. D: Appl. Phys.*, 2013, **46**, 024005.
- 23 S.-J. Lin, K.-C. Lee, J.-L. Wu and J.-Y. Wu, *Sol. Energy*, 2012, **86**, 2600.
- 24 S. D. Standridge, G. C. Schatz and J. T. Hupp, *J. Am. Chem. Soc.*, 2009, **131**, 8407.
- 25 S. D. Standridge, G. C. Schatz and J. T. Hupp, *Langmuir*, 2009, **25**, 2596.
- 26 M. D. Brown, T. Suteewong, R. S. S. Kumar, V. D'Innocenzo, A. Petrozza, M. M. Lee, U. Wiesner and H. J. Snaith, *Nano Lett.*, 2011, **11**, 438.
- 27 I.-K. Ding, J. Zhu, W. Cai, S.-J. Moon, N. Cai, P. Wang, S. M. Zakeeruddin, M. Grätzel,

- M. L. Brongersma, Y. Cui and M. D. McGehee, *Adv. Energy Mater.*, 2011, **1**, 52.
- 28 Y. Nakao and K. Soneb, *Chem. Commun.*, 1996, 897.
- 29 S. O. Obare, N. R. Jana and C. J. Murphy, *Nano Lett.*, 2001, **1**, 601.
- 30 J. Rodriguez-Fernandez, J. Perez-Juste, J. G. Abajo and L. M. Liz-Marzan, *Langmuir*, 2006, **22**, 7007.
- 31 J. H. Kim, M.-S. Kang, Y. J. Kim, J. Won, N.-G. Park and Y. S. Kang, *Chem. Commun.*, 2004, 1662.
- 32 L. M. Peter and K. G. U. Wijayantha, *Electrochim. Acta*, 2000, **45**, 4543.
- 33 J. Bisquert, G. Garcia-Belmonte, F. Fabregat-Santiago and A. Compte, *Electrochem. Commun.*, 1999, **1**, 429.